Redox Biology 46 (2021) 102118

Contents lists available at ScienceDirect

Redox Biology

journal homepage: www.elsevier.com/locate/redox

Ceruloplasmin deletion in myelinating glial cells induces myelin disruption and oxidative stress in the central and peripheral nervous systems

D.A. Santiago González [1], V.T. Cheli [1], S.L. Rosenblum [1], G. Denaroso, P.M. Paez [*]

Institute for Myelin and Glia Exploration, Department of Pharmacology and Toxicology, Jacobs School of Medicine and Biomedical Sciences, The State University of New York, University at Buffalo, Buffalo, NY, USA

ARTICLE INFO

Keywords:
Oligodendrocytes
Schwann cells
Iron
Ceruloplasmin
Myelination
Oxidative stress

ABSTRACT

Ceruloplasmin (**Cp**) is a ferroxidase enzyme that is essential for cell iron efflux and has been postulated to have a neuroprotective role. During the myelination process, oligodendrocytes (**OLs**) and Schwann cells (**SCs**) express high levels of Cp, but the role of this enzyme in glial cell development and function is completely unknown. To define the function of Cp in the myelination of the central and peripheral nervous systems, we have conditionally knocked-out Cp specifically in OLs and SCs during early postnatal development as well as in aged mice. Cp ablation in early OLs (postnatal day 2, P2) significantly affects the differentiation of these cells and the synthesis of myelin through the first four postnatal weeks. The total number of mature myelinating OLs was reduced, and the density of apoptotic OLs was increased. These changes were accompanied with reductions in the percentage of myelinated axons and increases in the *g*-ratio of myelinated fibers. Cp ablation in young myelinating OLs (P30 or P60) did not affect myelin synthesis and/or OL numbers, however, Cp loss in aged OLs (8 months) induced cell iron overload, apoptotic cell death, brain oxidative stress, neurodegeneration and myelin disruption. Furthermore, Cp deletion in SCs affected postnatal SC development and myelination and produced motor coordination deficits as well as oxidative stress in young and aged peripheral nerves. Together, our data indicate that Cp ferroxidase activity is essential for OLs and SCs maturation during early postnatal development and iron homeostasis in matured myelinating cells. Additionally, our results suggest that Cp expression in myelinating glial cells is crucial to prevent oxidative stress and neurodegeneration in the central and peripheral nervous systems.

1. Introduction

Ceruloplasmin (**Cp**) is a copper-containing ferroxidase enzyme that plays a key role in cellular iron export and has been postulated to have a neuroprotective function [1,2]. Cp cooperates with ferroportin, the ubiquitous and exclusive transmembrane protein responsible for cell iron export [3]. Cp antioxidant activity is necessary for preventing cellular oxidative damage to susceptible cell targets such as lipids and proteins [4], and more importantly, ensures the appropriate binding of extracellular iron to transferrin [5]. Therefore, Cp is essential for iron metabolism in every cell and tissue [6].

Absence of Cp in humans leads to iron accumulation and neurodegeneration in the CNS. Aceruloplasminemia is a hereditary disease caused by an autosomal recessive mutation in the Cp gene [7] and is characterized by progressive neurological symptoms including cerebellar ataxia, chorea, tremors, parkinsonism, and cognitive decline [7–9]. Psychiatric symptoms such as depression and anxiety have been shown to be the inaugural clinical manifestations in more than half of the patients with the disease [9]. Furthermore, pathological studies have revealed severe iron deposition in neurons and glial cells in the brain of aceruloplasminemic patients [10]. In advanced stages of the disease, neurodegeneration, iron accumulation and cell oxidative damage were found in all brain structures [5,11,12]. Also, neuronal and glial cell bodies show increased levels of redox-active iron with widespread lipid peroxidation and aberrant astrocytes show marked iron accumulation [13].

The CNS predominantly expresses the glycosylphosphatidylinositol-anchored form of Cp [14,15]. Cp from circulation does not appear to cross the blood-brain barrier, and that levels of soluble Cp in the cerebrospinal fluid are extremely low [16]). In the brain, Cp is present on the

* Corresponding author. Institute for Myelin and Glia Exploration, Department of Pharmacology and Toxicology, Jacobs School of Medicine and Biomedical Sciences, SUNY at Buffalo. NYS Center of Excellence, 701 Ellicott St., Buffalo, NY, 14203, USA.
E-mail address: ppaez@buffalo.edu (P.M. Paez).
[1] These authors made equivalent contributions.

https://doi.org/10.1016/j.redox.2021.102118
Received 30 July 2021; Received in revised form 20 August 2021; Accepted 23 August 2021
Available online 27 August 2021

surface of glial cells, including oligodendrocytes (**OLs**) and astrocytes [17]. Cp has been shown to play a central role in astrocytic iron metabolism by regulating iron efflux from these cells, thereby preventing their overload with potentially toxic transition metals [17]). RNA sequencing of the OL lineage found that plasma membrane-attached Cp is highly expressed by newly formed OL progenitor cells and that expression decreases as OLs become myelinating cells [18,19]. This suggests a role for Cp during early OL development. However, the function of Cp in OL development or in mature/aged myelinating cells is unknown. Schwann cells (**SCs**) also express high levels of membrane-anchored Cp and it has been suggested that this protein plays a central role in the regulation of iron levels in the peripheral nervous system [20,21]. The presence of Cp on the surface of SCs may reflect its involvement in iron transport during critical stages of SC development and/or the transfer of iron from one cell type to another in the peripheral nervous system. Although, the role of Cp in SCs development and/or myelination has yet to be explored.

In this work, we disrupted Cp expression in OLs and SCs using the *Cre-lox* system. This results in elimination of cell iron efflux via the Cp/ferroportin complex. Throughout early postnatal development Cp deletion severely affected OL development and function, this results in fewer myelinating OLs and brain hypomyelination. Although young OLs were found to be insensitive to the loss of Cp, aged OLs lacking Cp suffered iron overload and apoptotic cell death. Furthermore, knocking-out Cp in SCs affected the myelination of peripheral nerves and induced oxidative stress and motor coordination deficits. Overall, our results indicate the importance of Cp function in OL and SC iron metabolism as well as the myelination of the central and peripheral nervous systems. More importantly, our data reveal that abnormal iron efflux in glial cells can induce oxidative stress and neurodegeneration in the central and peripheral nervous system of aged animals.

2. Materials and methods

2.1. Transgenic mice

All animals used in this study were housed in the UB Division of Laboratory Animal Medicine vivarium. Procedures were approved by UB's Animal Care and Use Committee, and conducted in accordance with the guidelines in "Guide for the Care and Use of Laboratory Animals" from the National Institutes of Health. The Cp *tm1a(KOMP)Wtsi* "*knock-out first allele*" mouse [22]; Komp Mouse stock # 047193-UCD) was obtained from the Komp Mouse project at UC Davis. The Sox10-i*Cre*ERT2 mouse [23]; JAX stock # 027651), the NG2*Cre*ERT2 mouse [24]; JAX stock # 008538) and the ROSA26:FLPe knock-in transgenic strain [25]; JAX stock # 009086) were obtained from the Jackson Laboratory. A Cp-*floxed* (**$Cp^{f/+}$**) mouse was generated by crossing the $Cp^{tm1a(KOMP)Wtsi}$ mouse with the ROSA26:FLPe knock-in mouse, witch express the FLP1 recombinase driven by the Gt(ROSA)26Sor promoter. FLP1 mediated-recombination generated a Cp^{tmc1} "conditional ready allele" where the exon 7 of the Cp gene is flanked by *loxP* sites. Mice with the FRT deletion were backcrossed in C57Bl/6 for 10 generations. Experimental animals were generated by crossing the heterozygous *floxed* $Cp^{f/+}$ strain with the hemizygous Sox10i*Cre*ERT2 or NG2*Cre*ERT2 transgenic lines. For all the experiments presented in this work mice of either sex were used.

2.2. Mice treatments

P2 **Sox10-Cp^{KO}** ($Cp^{f/f}$, Sox10i*Cre*ERT2$^{Cre/-}$), **NG2-Cp^{KO}** ($Cp^{f/f}$, NG2*Cre*ERT2$^{Cre/-}$) and **control** (*Cre*-negative) littermates ($Cp^{f/f}$, Sox10i*Cre*ERT2$^{-/-}$ or NG2*Cre*ERT2$^{-/-}$) were intraperitoneally injected once a day for 5 consecutive days with 25 mg/kg tamoxifen (Sigma-Aldrich) and brain tissue and sciatic nerves were collected at P15 and P30. Furthermore, Sox10-Cp^{KO} and control littermates were injected intraperitoneally once a day for 5 consecutive days with 100 mg/kg tamoxifen at P30 and P60 and brain tissue/sciatic nerves were collected at P60 or P90, respectively. For studies in aged animals, 8-month-old Sox10-Cp^{KO} and control (*Cre* negative) littermates were injected with 100 mg/kg tamoxifen every other day for two weeks and brain tissue/sciatic nerves were collected at 10 and 12 months. A 25 mg/ml of tamoxifen stock solution was prepared by dissolving and sonicating tamoxifen in 19:1 autoclaved vegetable oil:ethanol. 25 mg/kg was the highest non-toxic dose for P2 pups and 100 mg/kg was the highest non-toxic dose for P30 and P60 mice. We have found that five consecutive tamoxifen injections starting at P2, P30 or P60 in mice double transgenic for Sox10i*Cre*ERT2 and the *Cre* reporter B6.Cg-Gt(ROSA)26Sortm9 (CAG-tdTomato)Hze/J (JAX stock # 007909) induced *Cre*-mediated recombination in more than 90% of callosal and cortical Olig2 positive cells [26,27]. Similarly, the maximum level of recombination in the NG2*Cre*ERT2 line (~80% of Olig2 positive cells) was achieved injecting P2 animals with five consecutive tamoxifen injections of 25 mg/kg [26,28].

2.3. Western blot

Protein samples were extracted from mouse brains and sciatic nerves using lysis buffer as described in Ref. [29]. Twenty μg of proteins per line were separated using NuPAGE® Novex® 4–12% Bis-Tris Protein Gels (Life Technologies). Electroblotted PDVF membranes were blocked over night at 4 °C with 5% non-fat milk and 0.1% tween-20 in PBS. Primary antibodies were diluted in blocking solution and membranes incubated 3 h at room temperature with agitation. Protein bands were detected by chemiluminescence using the Amersham ECL kit (GE Healthcare) with horseradish peroxidase-conjugated secondary antibodies (GE Healthcare) and scanned with a C-Digit Bot Scanner (LI-COR). Protein bands were quantified using the Image Studio™ Software (LI-COR). Primary antibodies: β actin (mouse; 1:1000; Sigma-Aldrich), CNP (mouse; 1:1000; Neo-Markes), MBP (mouse; 1:1000; Biolegend), NeuN (mouse; 1:1000; Millipore), neurofilament M (chicken; 1:1000; Millipore), PLP (rat; 1:500, AA3 - PLP/DM20) and p84 (mouse; 1:10,000; Genetex).

2.4. RT-PCR

RNA was isolated from brain tissue using Trizol (Life Technologies). The concentration and purity of the samples were evaluated by determining the ratio of absorbance at 260/280 nm. First-strand cDNA was prepared from 1 μg of total RNA using SuperScriptTM III RNase H-reverse transcriptase (Life Technologies) and 1 μg of oligo(dT). The mRNA samples were denaturized at 65 °C for 5min. Reverse transcription was performed at 50 °C for 55min and was stopped by heating the samples at 85 °C for 5min. The cDNA was amplified using specific primers and the PCR Platinum Super mix (Life Technologies). The PCR products were visualized on a SYBR Safe stained agarose gel and analyzed using a Gel Doc™ EZ System (Bio-Rad).

2.5. Immunohistochemistry

Animals were perfused with 4% of paraformaldehyde in PBS via the left ventricle and brains were post-fixed overnight in the same fixative solution at 4 °C. Coronal brain slices were obtained using a vibratome (Leica Biosystems, VT1000-S). Free-floating vibratome sections were treated with a blocking solution (2% goat serum, 1% Triton X-100 in PBS) for 2 h at room temperature and then incubated with the primary antibody overnight at 4 °C. Sections were then rinsed in PBS and incubated with Cy3 or Cy5 conjugated secondary antibodies (1:400; Jackson) for 2 h at room temperature. Brain slices were mounted in Superfrost Plus slides (Fisher) with mounting medium (Aquamount; Lerner Laboratories). The staining intensity for myelin proteins as well as the number of positive cells was assessed in the central area of the corpus callosum, between the midline and below the apex of the cingulum (0.6 mm^2), in the somatosensory cortex (0.6 mm^2) and in the

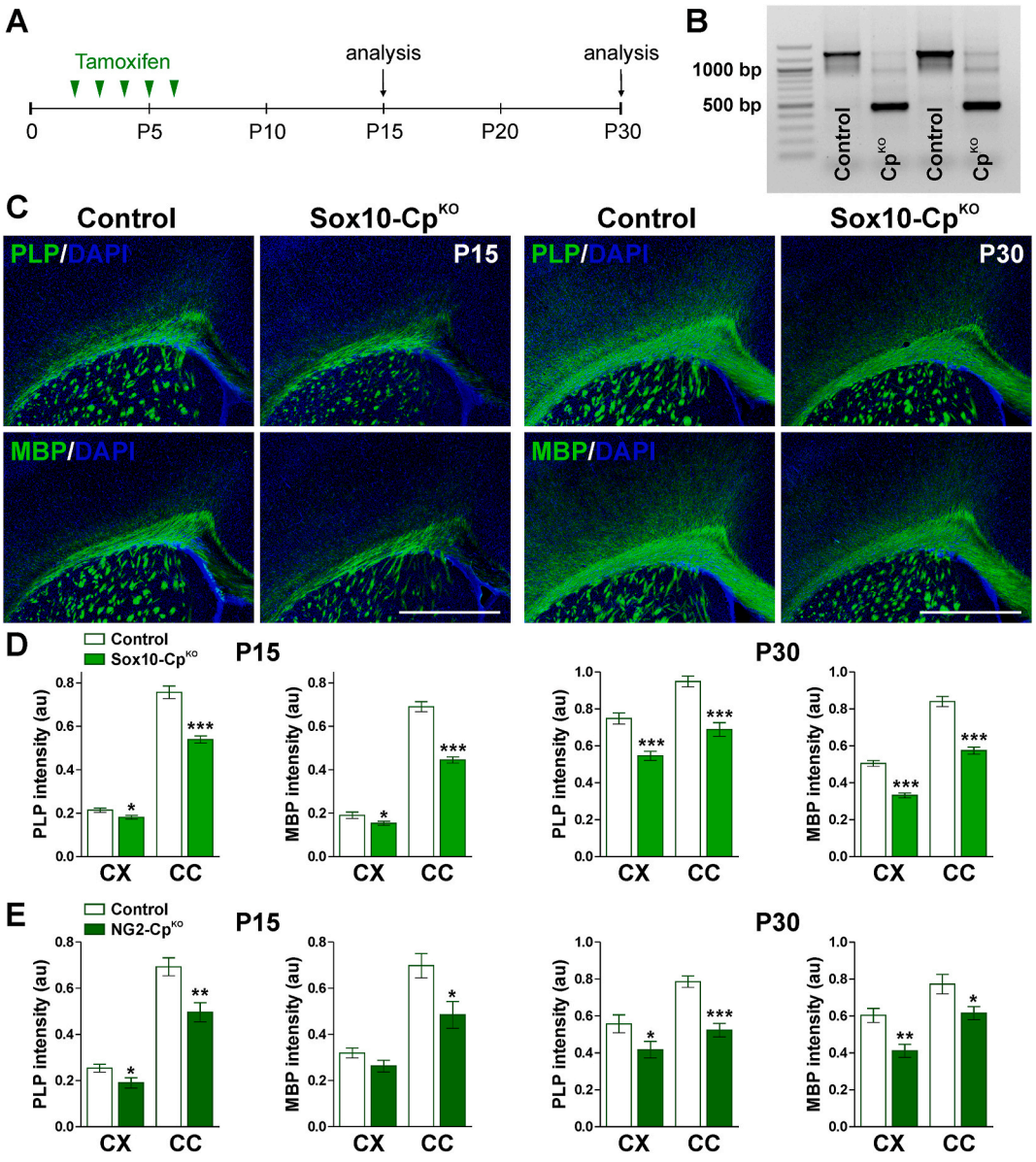

Fig. 1. *Expression of myelin proteins in the postnatal Cp^{KO} mouse.* (**A**) P2 Sox10-Cp^{KO}, NG2-Cp^{KO} and control (*Cre*-negative) littermates received 5 consecutive tamoxifen injections and brain tissue was collected at P15 and P30. (**B**) Semi-quantitative RT-PCR for Cp was performed at P15 with RNA isolated from the corpus callosum of control and Sox10-Cp^{KO} mice. (**C**) PLP and MBP immunostaining in the brain of control and Sox10-Cp^{KO} mice at P15 and P30. Scale bar = 180 μm. (**D and E**) PLP and MBP expression was quantified in Sox10-Cp^{KO} and NG2-Cp^{KO} brains by analyzing the integrated fluorescence intensity in the somatosensory cortex (**CX**) and central corpus callosum (**CC**). Values are expressed as mean ± SEM. *p < 0.05, **p < 0.01, ***p < 0.001 vs. respective controls.

dorsal/caudal striatum, immediately underneath the corpus callosum (0.6 mm^2) [30]; Figure 24). The integrated fluorescence intensity was calculated as the product of the area and mean pixel intensity using MetaMorph software (Molecular Devices). Fifteen slices per brain (50 μm each) were used and data represent pooled results from at least 4 brains per experimental group.

Mouse sciatic nerves were dissected and fixed overnight with 4% paraformaldehyde in PBS. Cross sections (10 μm thick) were obtained using a Clinical Cryostat (Leica Biosystems, CM1950) and mounted on Superfrost Plus slides (Fisher). Slices were treated with a blocking solution (5% goat serum, 1.5% bovine serum albumin, 2% Triton X-100) for 2 h at room temperature and then incubated with the primary antibody overnight (4 °C) and with the appropriate secondary antibodies (1:400; Jackson) for 2 h at room temperature. Twenty slices per sciatic nerve were analyzed and data represent pooled results from at least 4 sciatic nerves per experimental group. Antibodies: caspase-3 (mouse; 1:200; Cell Signaling), CC1 (mouse; 1:300; Calbiochem), Ki67 (rabbit; 1:250; Abcam), Ki67 (mouse; 1:250; BD Biosciences), MBP (mouse; 1:1000; Biolegend), NeuN (mouse; 1:100; Millipore), neurofilament L (chicken; 1:100; Millipore), neurofilament M (chicken, 1:2000; Biolegend), Olig2 (mouse and rabbit; 1:500; Millipore), P0 (chicken; 1:3000; Aves), PLP (rat; 1:250, AA3 - PLP/DM20), Sox2 (rabbit; 1:200; Millipore), s100β (rabbit; 1:800; Thermo Scientific) and 8-OHdG (mouse; 1:2000; StressMarq Biosciences).

2.6. Perls' histochemistry

Enhanced Perls' histochemistry was performed as described previously in Ref. [26]. Briefly, 20 μm coronal brain sections were incubated with 1% H_2O_2 in methanol for 15min and then with 2% potassium ferrocyanide (pH 1.0) overnight (Iron Stain Kit, Sigma-Aldrich). The reaction was enhanced for 30min with 0.025% 3,

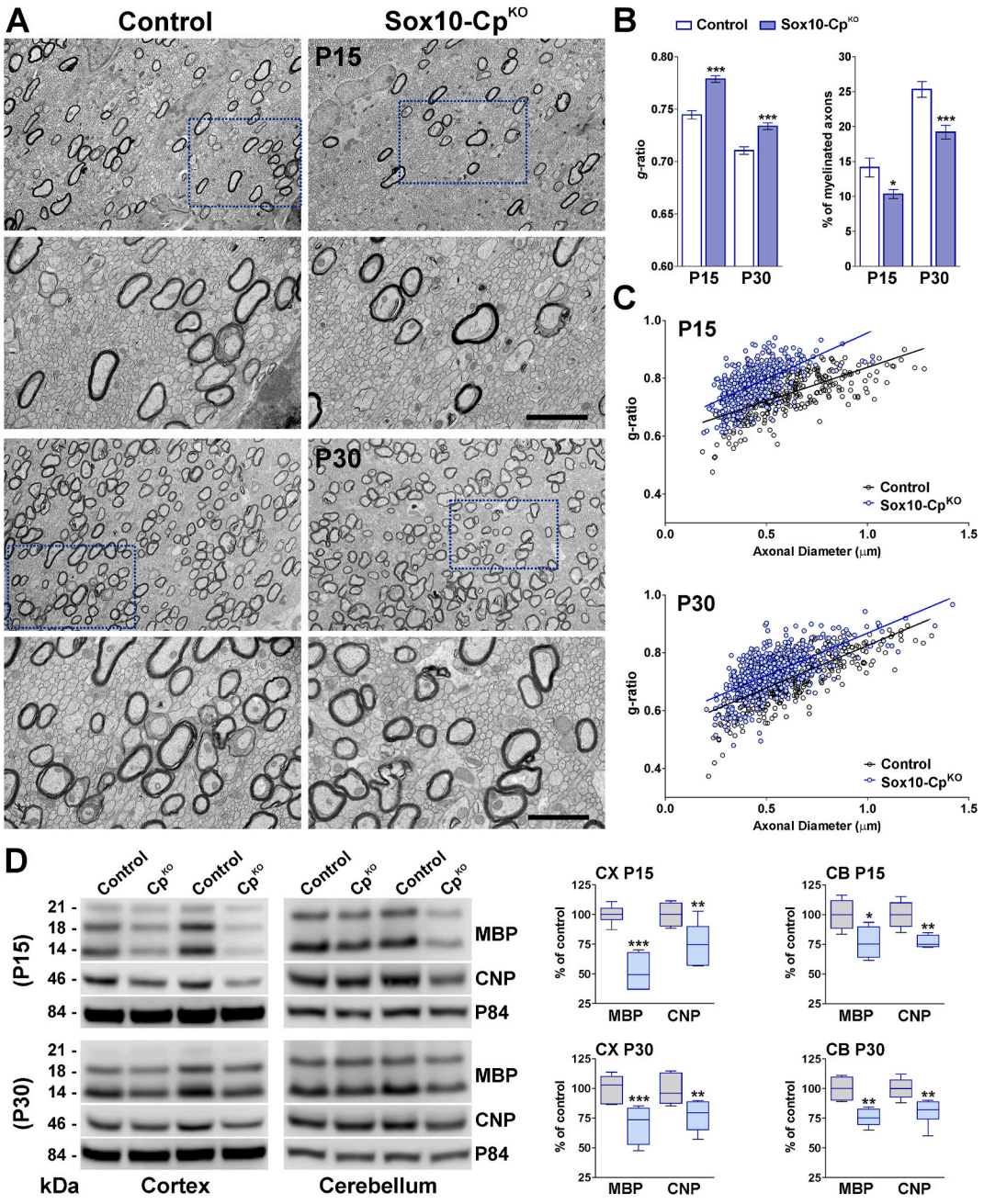

Fig. 2. ***Electron microscopy of the Cp^{KO} corpus callosum.*** (**A**) Electron micrographs of axons in the corpus callosum of control and Sox10-Cp^{KO} mice at P15 and P30. Scale bar = 8 μm upper panel; 2 μm lower panel. (**B**) Mean *g*-ratio values and percentage of myelinated axons. (**C**) Scatter plot of *g*-ratio values of myelinated axons at P15 and P30. Values are expressed as mean ± SEM. *p < 0.05, ***p < 0.001 versus control. (**D**) Representative western blots for MBP and CNP are shown. P84 was used as the internal standard and box-and-whisker plots are showing means ± SD. *p < 0.05, **p < 0.01, ***p < 0.001 vs. respective controls.

3′-diaminobenzidine-4Hl, 0.05% H_2O_2 and 0.005% $CoCl_2$ in 0.1 M PB. Then, tissue sections were dehydrated and mounted with Permount. The number of positive cells and the integrated staining intensity were assessed by MetaMorph software (Molecular Devices) in the central area of the corpus callosum, between the midline and below the apex of the cingulum (0.6 mm^2), in the somatosensory cortex including all cortical layers [30]; Figure 24) and in the substantia nigra [30]; Figure 52). Twelve slices per brain (20 μm each) were used and data represent pooled results from at least 4 brains per experimental group.

2.7. Electron microscopy

Mouse brains were perfused transcardially with 3% paraformaldehyde and 1% glutaraldehyde. The body of the corpus callosum at the anterior-dorsal level of the hippocampus was dissected and resin embedded. Sciatic nerves were fixed with 2% glutaraldehyde and then embedded in resin. Thin sections were stained with uranyl acetate and lead citrate and photographed with a FEI Tecnai^{TM} F20 transmission electron microscope as previously described [26,27]. The *g*-ratio and the percentage of myelinated axons were determined semi-automatically and blind to the genotype of the sample in 20 randomly selected fields per sample using MetaMorph software (Molecular Devices). For all experimental conditions, data represent pooled results from at least 4 mice.

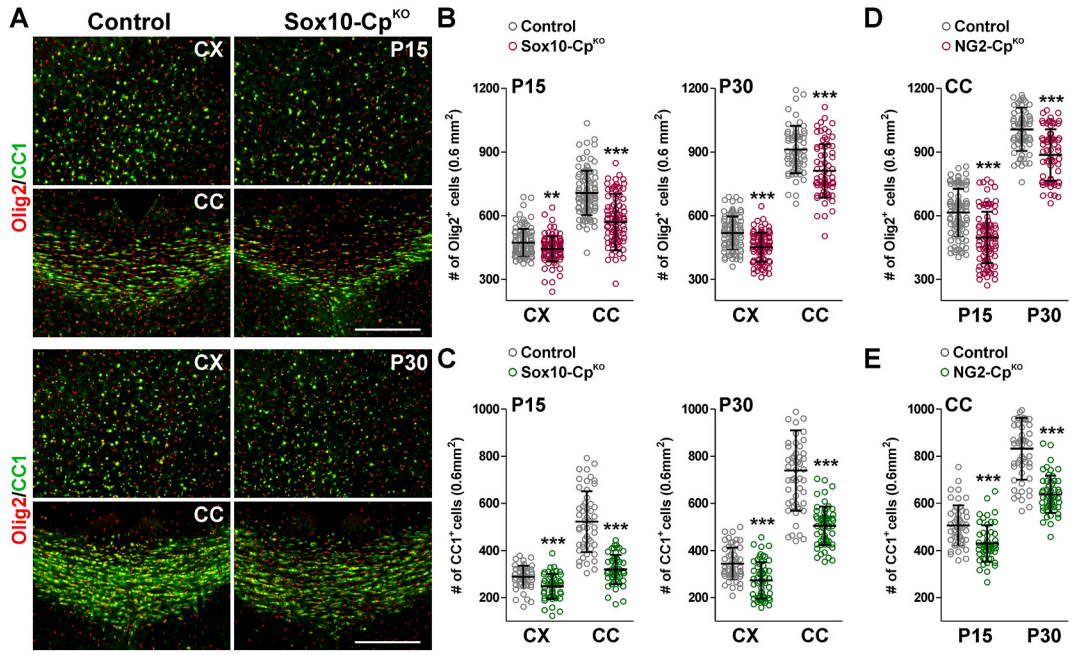

Fig. 3. *Oligodendrocyte numbers in Cp^{KO} brains during early development.* (**A**) Representative coronal sections from control and Sox10-Cp^{KO} brains immunostained for Olig2 and CC1 at P15 and P30. Scale bar = 90μm. (**B, C, D and E**) Olig2 and CC1-positive cells were quantified in the somatosensory cortex (**CX**) and central corpus callosum (**CC**) at P15 and P30. Scatter dot-plot graphs are showing single brain slices values plus mean ± SD. **p < 0.01, ***p < 0.001 vs. respective controls.

2.8. Rotarod

Coordinated motor activity was measured by a rotarod apparatus following the standard procedure of IMPReSS (International Mouse Phenotyping Resource of Standardised Screens). Mice were put on a rod rotating at 4 rpm. The speed of rotation was gradually increased up to 40 rpm in a 5min interval and the time elapsed before mice fell to the floor was measured. Each mouse was tested three times with 20min between each trial. At least 15 animals were tested in each experimental group.

2.9. Statistical analysis

Single between-group comparisons were made by the unpaired *t*-test (Student's t-test) using a confidence interval of 95%. Multiple comparisons were investigated by one-way ANOVA followed by Bonferroni's multiple comparison test to detect pair-wise between-group differences. All data sets were tested for normal distribution using the Kolmogorov-Smirnov test. For the analysis of *g*-ratio scatter plots, simple linear regression with a confidence interval of 95% was used. All statistical tests were performed in GraphPad Prism (GraphPad Software). A fixed value of $p < 0.05$ for two-tailed test was the criterion for reliable differences between groups. To minimize bias the quantification of all the experiments described in this work was performed blind to the sample genotype.

3. Results

3.1. The role of Cp in early oligodendrocyte development

In order to knock-out Cp in Sox10-or NG2-positive OLs, *Cre* activity was induced at P2 by intraperitoneal injection of tamoxifen. Cp conditional knock-out mice (**Sox10-Cp^{KO}**; Cp$^{f/f}$, Sox10i*Cre*ERT2$^{Cre/-}$) (**NG2-Cp^{KO}**, Cp$^{f/f}$, NG2*Cre*ERT2$^{Cre/-}$) and control (*Cre*-negative) littermates (**Control**; Cp$^{f/f}$, Sox10i*Cre*ERT2$^{-/-}$ or NG2*Cre*ERT2$^{-/-}$) were injected once a day for 5 consecutive days with tamoxifen, and brain tissue was collected at P15 and P30 for examination (Fig. 1A). Initially, *Cre* recombination was evaluated at P15 by RT-PCRs performed with total RNA isolated from the corpus callosum of tamoxifen treated Sox10-Cp^{KO} mice (Fig. 1B). A significant reduction in the wild-type Cp mRNA, and the presence of the expected truncated RNA messenger, indicate a high *Cre* recombination efficacy in our mouse model (Fig. 1B). To study the myelination of the postnatal Sox10-and NG2-Cp^{KO} brains, immunohistochemical experiments for myelin proteins were first performed in the somatosensory cortex and in the corpus callosum. A significant reduction in MBP and PLP fluorescent intensity was found in Sox10-and NG2-Cp^{KO} mice at both P15 and P30 (Fig. 1C, D and E). The corpus callosum was the most affected brain area showing a 30% average reduction in the synthesis of myelin proteins (Fig. 1C, D and E). To quantify the percentage of myelinated axons and the thickness of the myelin sheath, the body of the corpus callosum was analyzed by electron microscopy. A key measure of white matter health is the *g*-ratio, which is defined as the ratio between the inner axon radius and the outer myelinated axon radius. Suggesting a reduction in the myelin thickness, myelinated axons from Sox10-Cp^{KO} mice showed a significant increase in *g*-ratio values (Fig. 2A, B and C). As showed in Fig. 2C, axons of all sizes were affected, and these changes were accompanied with declines in the percentage of myelinated axons (Fig. 2B). These data were supported by Western blot experiments for myelin proteins performed with protein samples isolated from the cortex and cerebellum of control and Sox10-Cp^{KO} mice. In agreement with the results described above, the expression levels of MBP and CNP were significantly reduced in Sox10-Cp^{KO} mice at both P15 and P30 (Fig. 2D).

Oligodendrocyte numbers were also analyzed in Sox10 and NG2-Cp^{KO} brains using oligodendroglia-specific markers such as Olig2 and CC1. The cortex of Sox10-Cp^{KO} mice showed small reductions in the amount of Olig2 and CC1-positive cells (Fig. 3A, B and C). However, both the total number of OLs (Olig2-positive cells) and the density of mature myelination OLs (CC1-positive cells) decreased more than 30% in the corpus callosum of Sox10-Cp^{KO} animals at P15 and P30 (Fig. 3A, B and C). NG2-Cp^{KO} animals also showed a prominent reduction in the density of Olig2 and CC1-expressing cells in the corpus callosum at both time-points (Fig. 3D and E). To examine how the loss of Cp affects the proliferation and survival of immature OLs, the Olig2 antibody was combined with Ki67, a marker of cell proliferation, and with Sox2, a transcription factor expressed by newly generated OLs. An increase in

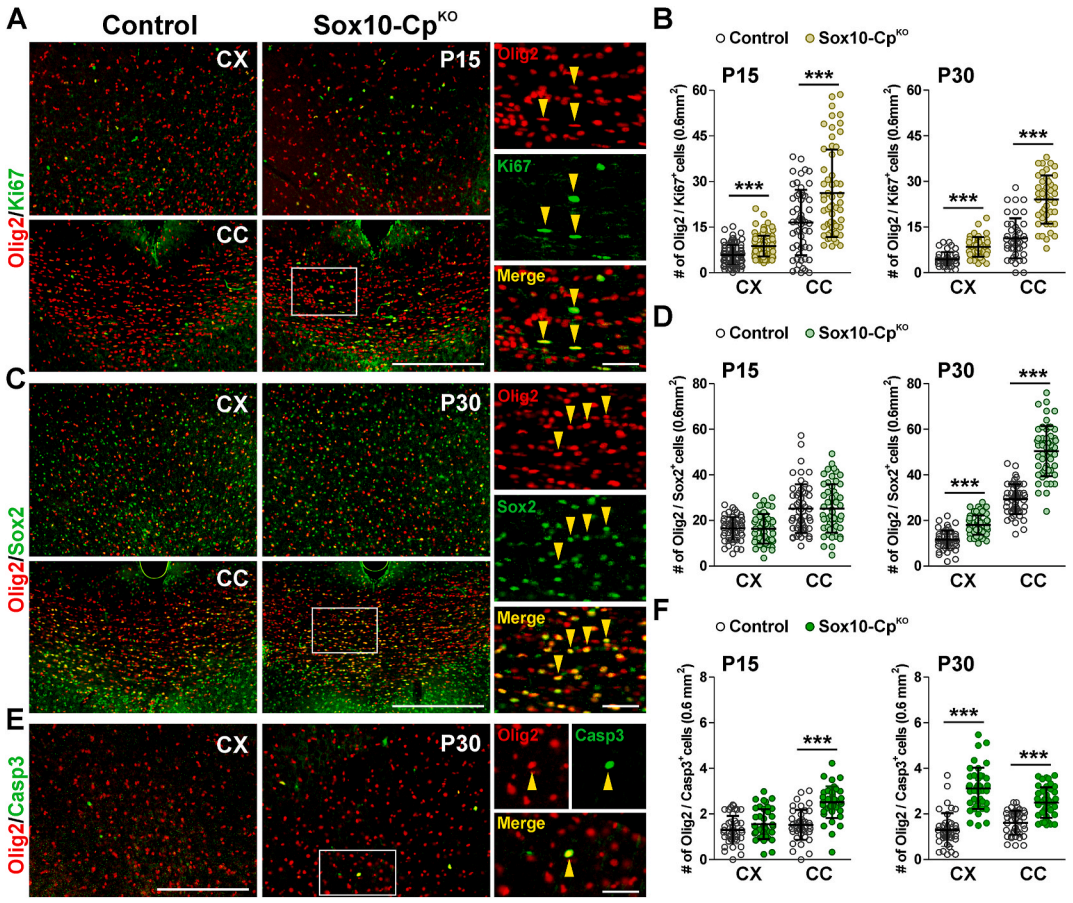

Fig. 4. *Proliferation and survival of Cp-deficient oligodendrocytes.* (**A, C and E**) Representative coronal sections from control and Sox10-Cp^{KO} brains at P15 and P30 immunostained for Olig2, Ki67, Sox2 and caspase-3. Scale bar = 90 μm. Arrowheads in high magnification insets indicate examples of double positive cells that were selected for the analysis. Scale bar = 30μm. (**B, D and F**) Olig2/Ki67, Olig2/Sox2 and Olig2/Casp3 double-positive cells were quantified in the somatosensory cortex (**CX**) and central corpus callosum (**CC**) at P15 and P30. Scatter dot-plot graphs are showing single brain slices values plus mean ± SD. ***p < 0.001 vs. respective controls.

the number of Olig2/Ki67 double-positive cells was found in the cortex and corpus callosum of Sox10-Cp^{KO} mice at P15 and P30 (Fig. 4A and B). These brain areas showed no significant changes in the quantity of Olig2/Sox2 double-positive cells at P15 (Fig. 4D), but at P30, Sox10-Cp^{KO} brains presented a significant rise in the amount of newly generated OLs (Fig. 4C and D). Moreover, a specific antibody against the activated form of caspase-3 was used to evaluate apoptotic cell death. Sox10-Cp^{KO} mice showed a significant increase in apoptotic OLs (Olig2/Casp3 double-positive cells), particularly in the corpus callosum at P15 and in the cortex and corpus callosum at P30 (Fig. 4E and F).

Similar experiments were conducted in juvenile mice to study whether Cp deletion in young OLs affects myelin synthesis and/or OL numbers. For this set of experiments, Sox10-Cp^{KO} and control animals were injected with tamoxifen at P30 or P60 and brain samples were collected at P60 or P90, respectively (Fig. 5A). The expression of MBP and PLP in P60 animals was normal in all the brain areas analyzed (Fig. 5B and C). In the same line, no statistical differences were detected in the number of Olig2-positive cells (Fig. 5E and F). At this time-point, only a small reduction in CC1-expressing cells was noticed in the cortex of Cp-deficient mice (Fig. 5E and G). Suggesting that Cp is not relevant for the function of mature myelinating OLs of the young CNS, the expression of MBP and PLP in P90 Sox10-Cp^{KO} mice was also equivalent to controls (Fig. 5B and D). Additionally, no significant differences in the number of Olig2 or CC1-positive cells were found at this age (Fig. 5F and G).

3.2. Cp ablation in aged oligodendrocytes

Cp plays a key function in cellular iron metabolism, and has been postulated to have a neuroprotective role in the adult and aging CNS. In this context, we have evaluated how the loss of Cp affects OLs in the aged mouse brain. For this group of experiments, control and Sox10-Cp^{KO} mice were treated with tamoxifen at 8 months of age, and OL numbers and myelination were analyzed two and four months later (10 M and 12 M, respectively) (Fig. 6A). At 10 months, PLP and MBP fluorescent intensity was slightly reduced in Sox10-Cp^{KO} mice (**data not shown**). However, these changes were more prominent at 12 months of age. At this time-point, Sox10-Cp^{KO} animals lost more than 20% of PLP expression in all brain structures and exhibited a ~50% reduction in MBP levels in the central and lateral areas of the corpus callosum (Fig. 6B and C). Furthermore, electron microscopy experiments revealed a clear reduction in the myelin thickness as well as in the percentage of myelinated axons in the corpus callosum of Sox10-Cp^{KO} mice at both time-points (Fig. 6D, E and F). In accordance with these results, Western blot experiments exposed a reduction in myelin protein expression in the cortex of aged Sox10-Cp^{KO} brains (Fig. 6G).

Examination of the OL population revealed a substantial decrease in the number of Olig2-and CC1-positive cells in 10 and 12 month-old Sox10-Cp^{KO} animals (Fig. 7A–D). These declines were found to be more prominent in both the cortex and the corpus callosum of 12-month-old Sox10-Cp^{KO} mice (Fig. 7A–D). We did not find differences in the number of proliferating OLs at 10 months (Fig. 7G), however, a significant increase in Olig2/Ki67 expressing cells was detected in the

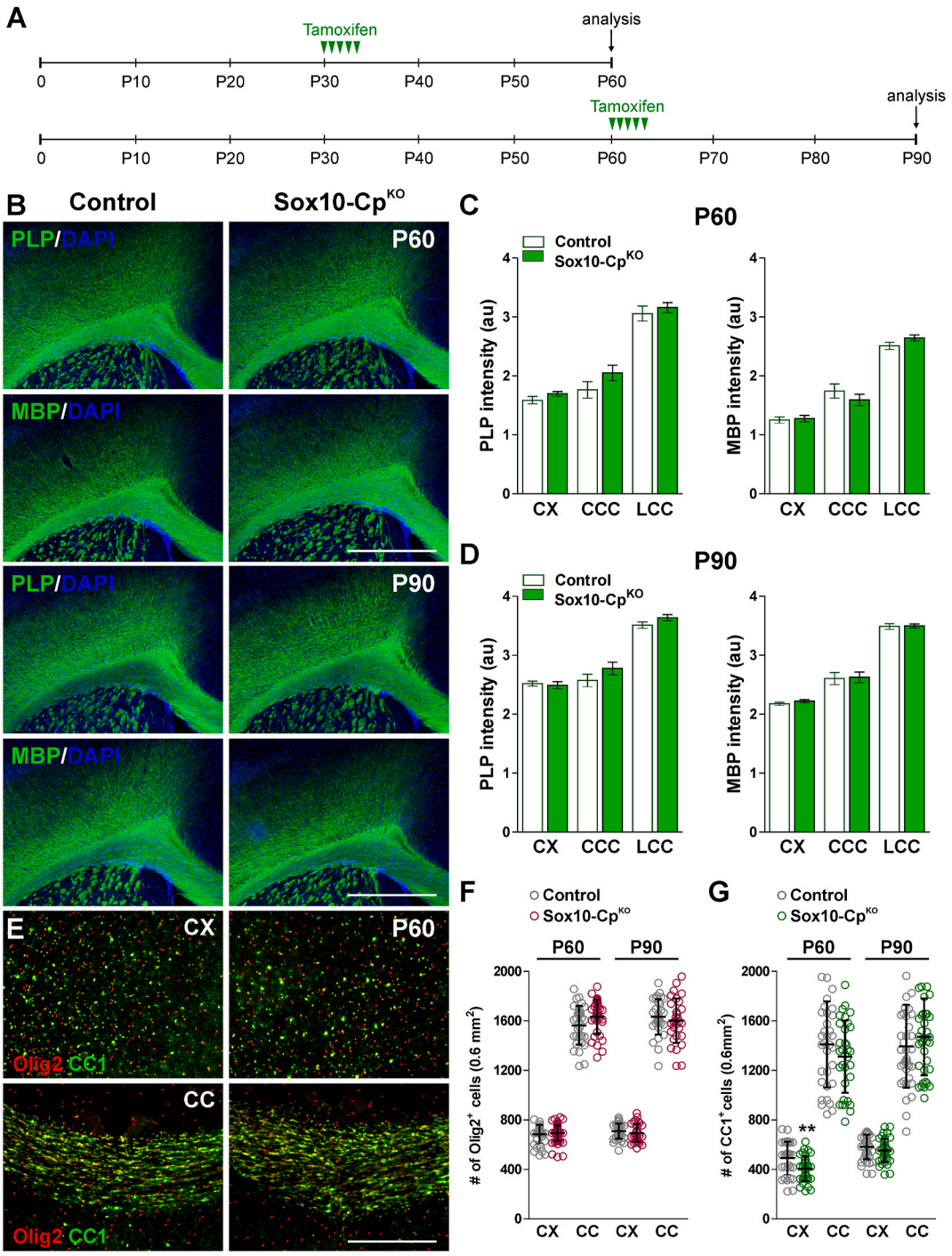

Fig. 5. *Oligodendrocyte numbers and myelination in the Cp^{KO} adult brain.* (**A**) Five tamoxifen injection were given to P30 and P60 Sox10-Cp^{KO} and control (*Cre*-negative) animals and brain samples were collected at P60 and P90. (**B**) PLP and MBP immunostaining in the brain of control and Sox10-Cp^{KO} mice at P60 and P90. Scale bar = 180 μm. (**C and D**) PLP and MBP expression was quantified by analyzing the integrated fluorescence intensity in the somatosensory cortex (**CX**) and central and lateral corpus callosum (**CCC** and **LCC,** respectively). Values are expressed as mean ± SEM. (**E**) Brain coronal sections from control and Sox10-Cp^{KO} brains immunostained for Olig2 and CC1 at P60. Scale bar = 90 μm. (**F and G**) Olig2 and CC1-positive cells were quantified in the somatosensory cortex (**CX**) and central corpus callosum (**CC**) at P60 and P90. Scatter dot-plot graphs are showing single brain slices values plus mean ± SD. **p < 0.01 vs. respective controls.

cortex and subventricular zone of 12 month-old Sox10-Cp^{KO} mice (Fig. 7E and G). Suggesting that Cp deletion is detrimental for mature OLs of the aged brain, we found a clear rise in the number of apoptotic myelinating OLs (CC1/Casp3 double-positive cells) in the cortex and corpus callosum of Sox10-Cp^{KO} mice at 10 and 12 months of age (Fig. 7F and H).

3.3. The function of Cp in oligodendrocyte iron metabolism

To measure intracellular iron quantities in different brain cells, the enhanced Perls' histochemistry technique was performed in brain tissue slices from P30, P90 and 12-month-old Sox10-Cp^{KO} mice. At P30 and P90, the density and staining intensity of iron-positive OLs in Sox10-Cp^{KO} cortex and corpus callosum were similar to controls (Fig. 8A, B and C). However, the cortex and corpus callosum of 12 month-old Sox10-

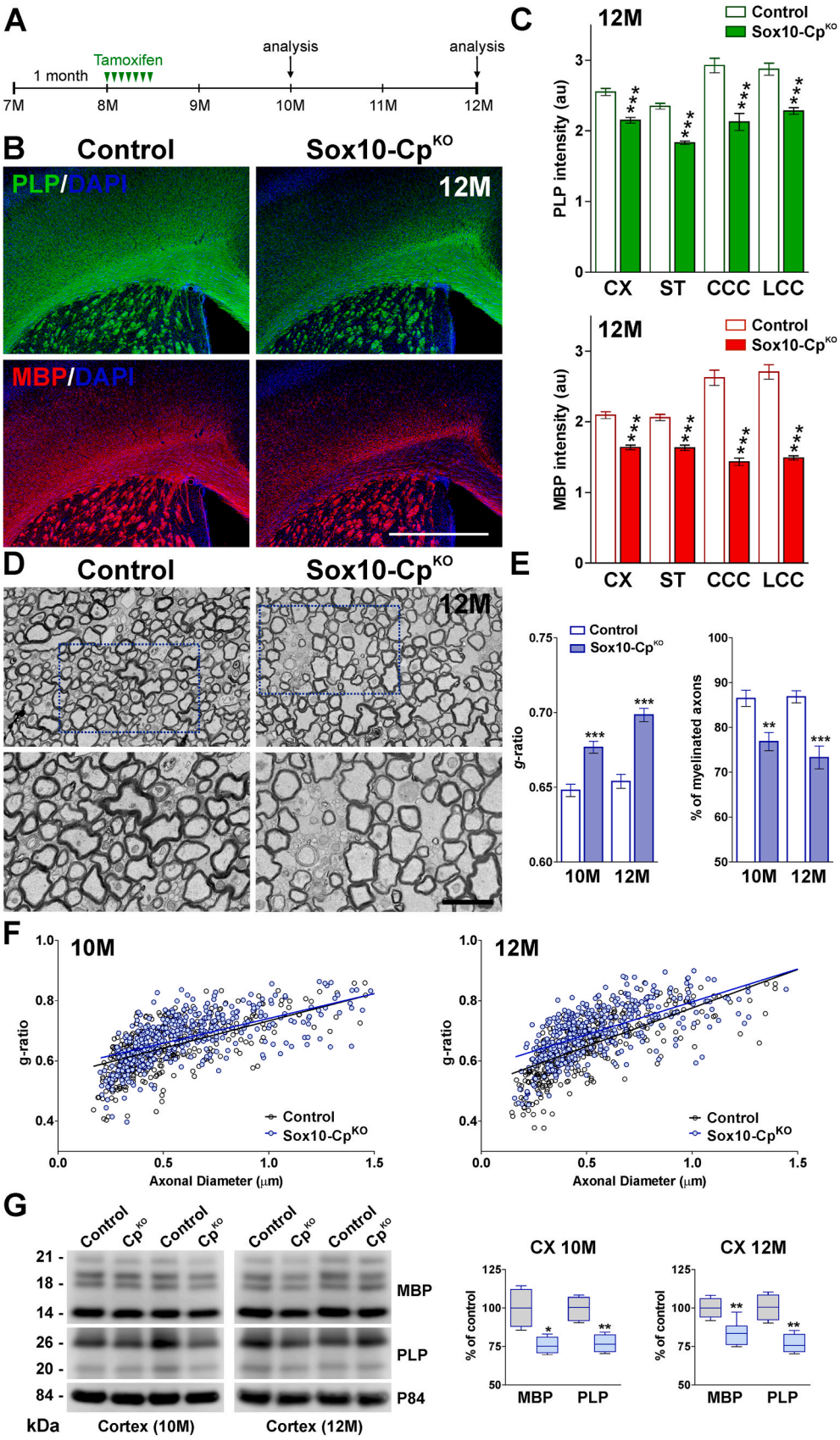

Fig. 6. *Myelin synthesis in the aged Cp^{KO} CNS.* (**A**) 8-month-old Sox10-Cp^{KO} and control (*Cre*-negative) littermates were injected with tamoxifen every other day during two weeks, and brain tissue was collected at 10 and 12 months (**10M** and **12M**). (**B**) PLP and MBP immunostaining in the brain of control and Sox10-Cp^{KO} mice at 12 M. Scale bar = 180 μm. (**C**) PLP and MBP expression was quantified by analyzing the integrated fluorescence intensity in the somatosensory cortex (**CX**), striatum (**ST**) and central and lateral corpus callosum (**CCC** and **LCC,** respectively). Values are expressed as mean ± SEM. ***p < 0.001 vs. respective controls. (**D**) Electron micrographs of axons in the corpus callosum of control and Sox10-Cp^{KO} mice at 12 M. Scale bar = 8 μm upper panel; 2 μm lower panel. (**E**) Mean *g*-ratio values and percentage of myelinated axons at 10 M and 12 M. (**F**) Scatter plot of *g*-ratio values of myelinated axons. Values are expressed as mean ± SEM. **p < 0.01, ***p < 0.001 versus control. (**G**) Western blots for MBP and PLP are shown. P84 was used as the internal standard and box-and-whisker plots are showing means ± SD. *p < 0.05, **p < 0.01 vs. respective controls.

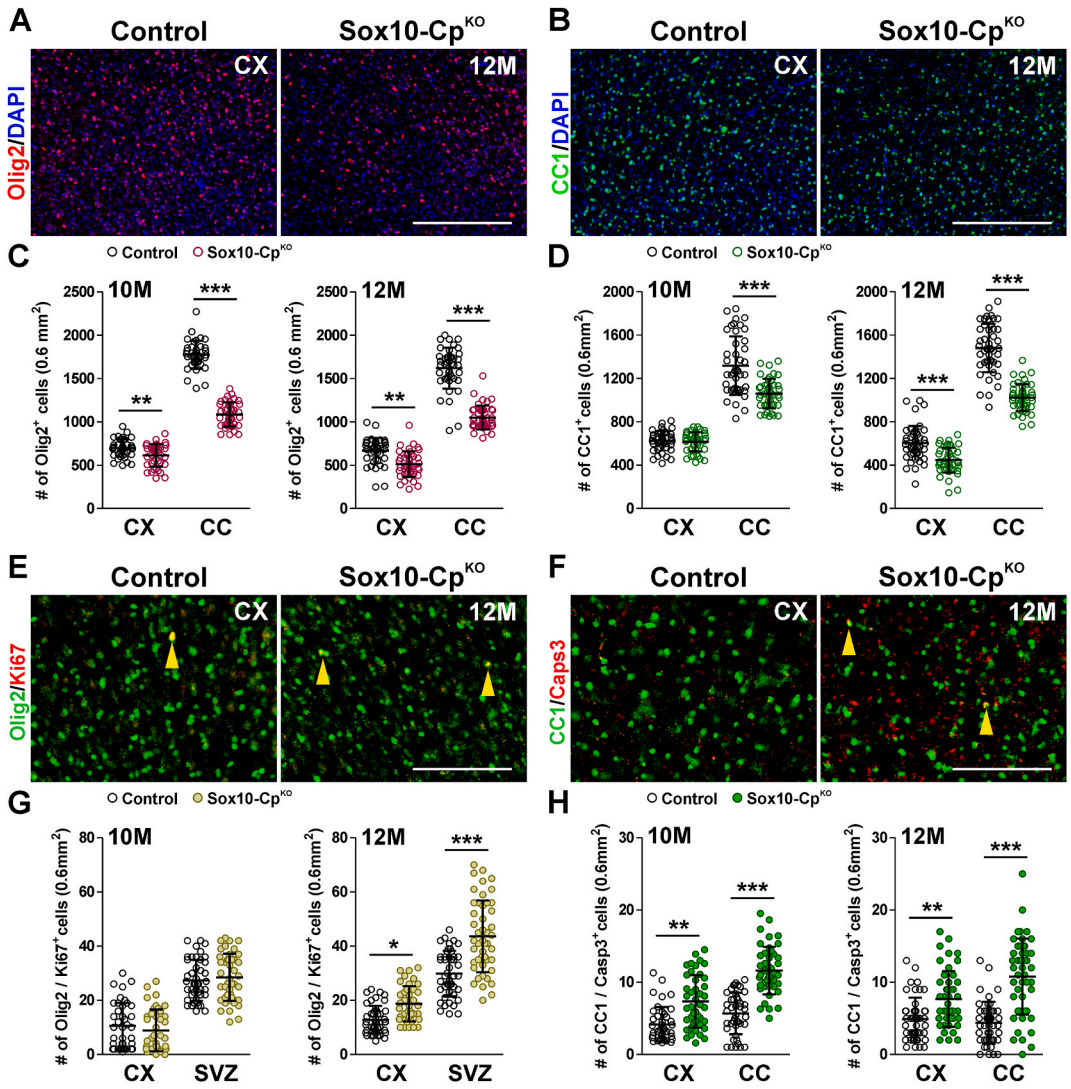

Fig. 7. *Oligodendrocyte quantities in aged Cp^{KO} brains.* (**A and B**) Representative coronal sections from control and Sox10-Cp^{KO} brains immunostained for Olig2 and CC1 at 12 M. Scale bar = 90 μm. (**C and D**) Olig2 and CC1-positive cells were quantified in the somatosensory cortex (**CX**) and central corpus callosum (**CC**) at 10 M and 12 M. (**E and F**) Representative coronal sections from control and Sox10-Cp^{KO} brains immunostained for Olig2, Ki67 and caspase-3 at 12 M. Scale bar = 40 μm. (**G and H**) Olig2/Ki67 and CC1/Casp3 double-positive cells were quantified in the somatosensory cortex (**CX**), sub-ventricular zone (**SVZ**) and central corpus callosum (**CC**) at 10 M and 12 M. Scatter dot-plot graphs are showing single brain slices values plus mean ± SD. *p < 0.05, **p < 0.01, ***p < 0.001 vs. respective controls.

Cp^{KO} animals showed a clear intensification in the number and staining intensity of iron-positive cells (Fig. 8A, B and C). Suggesting an OL-specific iron overload, the average Perls' staining intensity in cortical neurons and in the substantia nigra was found to be normal (Fig. 8A and D).

We next determined whether OL iron overload was accompanied by brain oxidative stress and neuronal cell loss. To test for neuron densities in the somatosensory cortex, we performed immunostainings against the neuronal nuclear antigen NeuN using brain sections from P30, P90 and 12-month-old Sox10-Cp^{KO} mice (Fig. 9A and B). A significant reduction of NeuN-positive neurons was observed in the somatosensory cortex of Sox10-Cp^{KO} mice at 12 months of age (Fig. 9A and B); consequently, the cortical thickness of Sox10-Cp^{KO} animals was significantly reduced (Fig. 9A and B). We additionally quantified the expression of neurofilament L in the same brain area and found a clear decline in the fluorescent intensity for this protein in all cortical layers (Fig. 9A and B). Interestingly, the somatosensory cortex of Sox10-Cp^{KO} mice at 12 months of age presented "neurodegenerative patches" characterized by reduced NeuN expression and increased cellularity (DAPI signal) (Fig. 9A). Moreover, the levels of NeuN and neurofilament L were found to be reduced in Western blot experiments performed with cortical samples from 12-month-old Sox10-Cp^{KO} mice (Fig. 9C). In contrast, the density of NeuN-positive cells, cortical thickness and expression of neurofilament L were found to be normal in P30 and P90 Sox10-Cp^{KO} brains (Fig. 9B). Next, we immunolabeled somatosensory cortex sections of Sox10-Cp^{KO} mice to examine oxidative DNA and RNA damage in OLs and neurons (Fig. 9D and E). 8-hydroxylated guanin species such as 8-hydroxy-2′-deoxyguanosine (8-OHdG) are repair products of oxidized guanine lesions and have been used as markers for DNA and RNA damage associated to oxidative stress [31]. No changes were appreciated at P30 or at P90; however, we detected an increase in 8-OHdG DNA and RNA oxidation in Olig2-and NeuN-positive cells in Sox10-Cp^{KO} mice at 12 months of age (Fig. 9D and E). Additionally, several antioxidant enzymes were analyzed in the brain cortex of 12-month-old Sox10-Cp^{KO} mice by semiquantitative RT-PCR (Fig. 9F). The expression of the stress-induced heme oxygenase-1 (**HO-1**) was similar to controls, but the levels of the superoxide dismutase (**SOD**) and the glutathione peroxidase (**GPX**) were increased in the cortex of aged Cp-deficient mice (Fig. 9F).

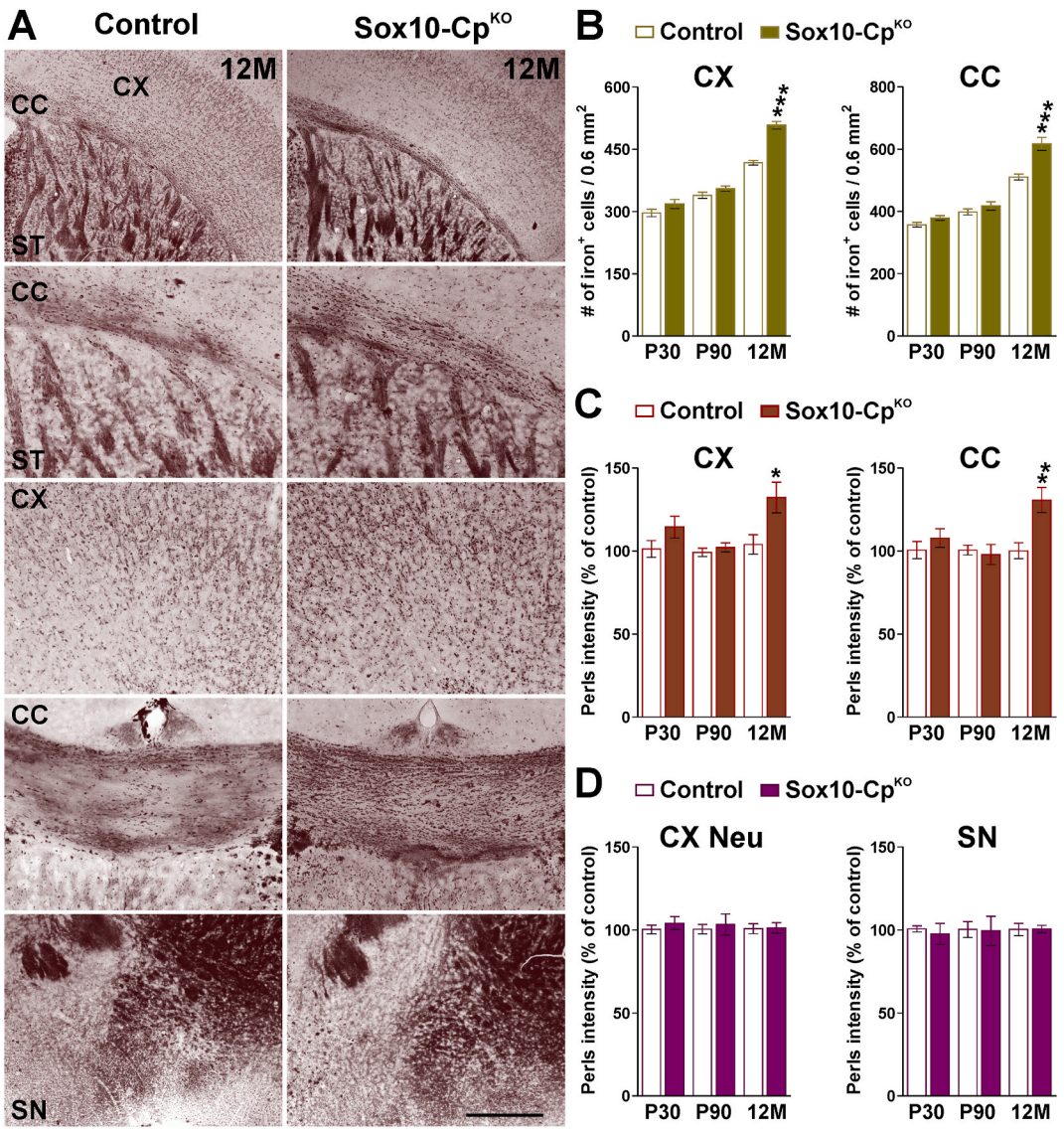

Fig. 8. ***Perls' staining in the Cp^{KO} CNS.*** (**A**) Perls' staining in representative brain coronal sections collected from control and Sox10-Cp^{KO} mice at 12 M. Scale bar = 180 μm upper panels; 90 μm lower panels. (**B and C**) Perls'-positive OLs and the average intensity staining per cell were quantified in the somatosensory cortex (**CX**) and central corpus callosum (**CC**) at P30, P90 and 12 M. (**D**) Perls' intensity staining was quantified in cortical neurons (**CX Neu**) and substantia nigra (**SN**) at the same time-points. Values are expressed as mean ± SEM. *p < 0.05, **p < 0.01, ***p < 0.001 vs. respective controls.

3.4. Cp and iron efflux in the peripheral nervous system

We conducted a series of EM experiments in sciatic nerves isolated from Sox10-Cp^{KO} mice injected with tamoxifen during the first postnatal week. At P15 and P30, these animals displayed an important increase in the mean *g*-ratio of myelinated axons as well as a significant reduction in the percentage of myelinated axons (Fig. 10A and C-F). Changes in *g*-ratios were equal among axons of all sizes (Fig. 10D). Parallel experiments were also performed in P90 sciatic nerves from Sox10-Cp^{KO} mice injected with tamoxifen at P60. Knocking-out Cp in adult myelinating SCs reduced myelin thickness and the percentage of myelinated axons (Fig. 10B, C and E-G). Next, we performed a series of Western blot experiments in Sox10-Cp^{KO} sciatic nerves to evaluate myelin proteins synthesis (Fig. 11A and B). In agreement with the EM data, the expression levels of MBP, CNP and PLP were significantly lower in Sox10-Cp^{KO} sciatic nerves at both P15 and P30 (Fig. 11A). Importantly, these changes were more prominent in P30 samples where the decrease in the expression of myelin proteins was greater than 25% (Fig. 11A). Similar results were detected in older Sox10-Cp^{KO} animals. Sciatic nerves isolated from P90 Sox10-Cp^{KO} mice (injected with tamoxifen at P60) and 12 month-old Sox10-Cp^{KO} animals (injected with tamoxifen at 8 months) showed an average 30% reduction in all three myelin proteins (Fig. 11B). These results were corroborated by immunohistochemistry in 12 month-old Sox10-Cp^{KO} sciatic nerves (Fig. 11D and E). Sox10-Cp^{KO} sciatic nerves presented less MBP and P0 fluorescent intensity than controls and displayed a clear increase in 8-OHdG DNA and RNA oxidation (Fig. 11D and E). Finally, motor coordination was measured across genotypes using the rotarod test. At P30, Sox10-Cp^{KO} mice exhibited an important reduction in the latency to fall off the rotarod (Fig. 11C); these changes were also observed in P90 Sox10-Cp^{KO} animals that were treated with tamoxifen at P60 (Fig. 11C).

4. Discussion

Cp has been associated with a set of neurodegenerative diseases called neurodegeneration with brain iron accumulation. Null mutations of the Cp gene in humans (aceruloplasminemia) result in iron accumulation in various organs including the CNS [7,32–34]. Iron accumulation

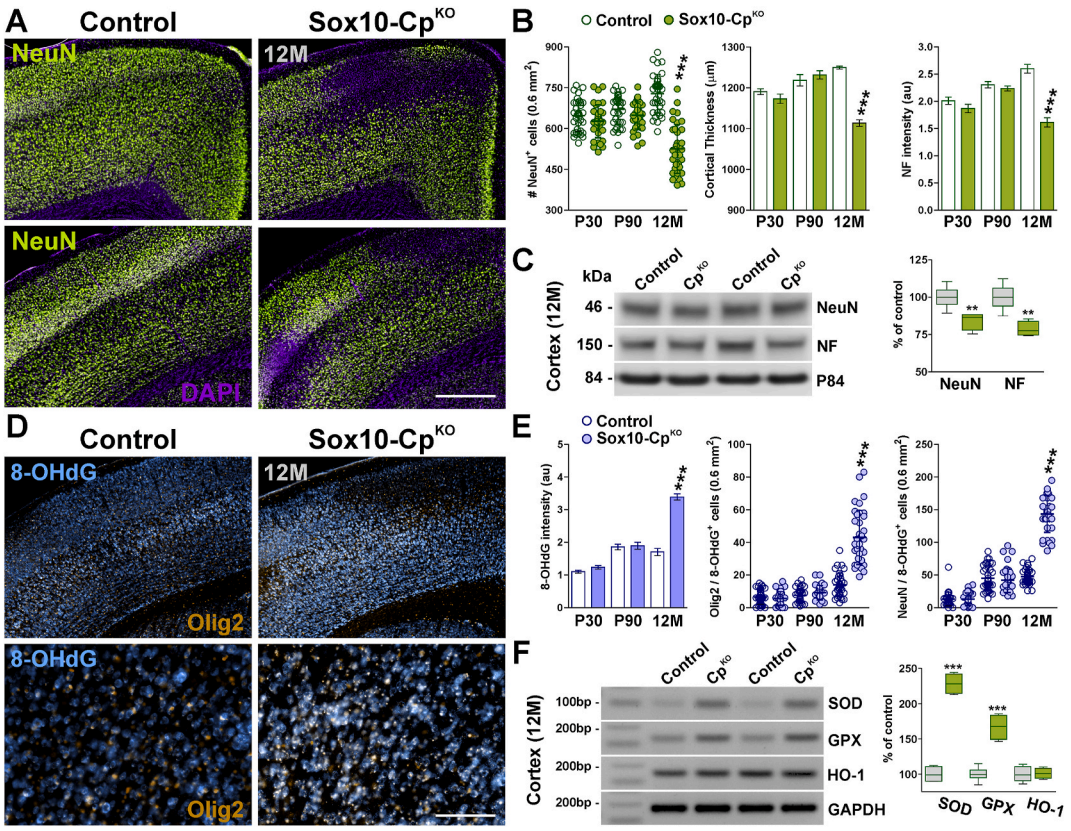

Fig. 9. *Neuronal densities and oxidative stress in Cp^{KO} brains.* (**A and D**) Representative coronal sections from control and Sox10-Cp^{KO} brains immunostained for NeuN, Olig2 and 8-OHdG at 12 M. (A) scale bar = 180 µm; (D) scale bar = 180 µm upper panel; 90 µm lower panel. (**B**) NeuN-positive cells, cortical thickness and neurofilament L fluorescence intensity were quantified in the somatosensory cortex at P30, P90 and 12 M. (**C**) Representative western blots for NeuN and neurofilament M at 12 M. P84 was used as the internal standard and box-and-whisker plots are showing means ± SD. **p < 0.01 vs. respective controls. (**E**) 8-OHdG fluorescence intensity and Olig2/8-OHdG and NeuN/8-OhdG double-positive cells were quantified in the somatosensory cortex at P30, P90 and 12 M. Scatter dot-plot graphs are showing single brain slices values plus mean ± SD. ***p < 0.001 vs. respective controls. (**F**) Semi-quantitative RT-PCRs for superoxide dismutase (**SOD**), glutathione peroxidase (**GPX**) and heme oxygenase-1 (**HO-1**) were performed at 12 M with RNA isolated from the cortex of control and Sox10-Cp^{KO} mice. GAPDH was used as the internal standard and data are summarized based on the relative spot intensities and plotted as percent of controls. Box-and-whisker plots are showing means ± SD. ***p < 0.001 vs. respective controls.

and neurodegeneration in this condition occurs between 45 and 55 years of age [35–37]. These patients usually experience neurological symptoms such as cerebellar ataxia, chorea, tremors, cognitive decline, and even parkinsonism [7–9]. Full knock-out mice for Cp also show iron accumulation in the CNS [4,38]. For example, the cerebellum of aged Cp knock-out mice displays reduced numbers of astrocytes with increased ferritin expression and iron accumulation [39]).

We have detected important reductions in the total number of OLs and in the density of mature myelinating OLs in Sox10- and NG2-Cp^{KO} mice during the first four postnatal weeks. These changes significantly affect myelin synthesis, the percentage of myelinated axons and the *g*-ratio of myelinated fibers. We have also found more proliferating and apoptotic OLs in Sox10-Cp^{KO} brains. However, the ablation of Cp in oligodendroglial cells after the peak of myelination (P30 and P60) did not affect OL proliferation, survival and/or myelination. These results suggest that Cp activity is essential for OL maturation and subsequent myelination during early development and highlight the necessity of OLs to export iron in the developing brain. Cp deletion in early OLs can potentially reduce iron efflux and make these cell more susceptible to oxidative stress; consequently, excess iron and disrupted iron homeostasis may leave immature OLs in an arrested state of proliferation, blocking differentiation and inducing apoptotic cell death.

[40] have shown that Cp is expressed by astrocytes and neurons; a similar ferroxidase called hephaestin is present in OLs. However, Cp is highly expressed in immature OLs and its expression decreases as these cells become mature myelinating OLs [18,19]. Actually, OL iron homeostasis was found to be normal in mice carrying a mutation in the hephaestin gene which eliminated the activity of this Cp-homolog ferroxidase enzyme [40]. Importantly, Cp was drastically upregulated in these OLs; in fact, the level of Cp activity in white matter OLs was four-fold higher than controls [40]. These data indicate that hephaestin and Cp likely collaborate to prevent iron accumulation in OLs and, more importantly, suggest a central role for Cp in OL iron balance during early development. However, the functional relationship between these proteins in OL iron homeostasis and how the expression of these proteins is controlled in the brain is not known. An understanding of these aspects will significantly improve our knowledge of the role of Cp in immature and aged OLs.

Several studies have shown that Cp is required for iron efflux in astrocytes and neurons [17]; 2006; [4], and that Cp activity protects astrocytes and neurons from free radical injury [4]. Myelinating OLs are also very susceptible to oxidative stress [41,42]. OLs can be easily damaged and are particularly sensitive to both hypoxia and oxidative stress, especially during their terminal differentiation and throughout the myelination process [43]). Iron overload and oxidative stress most likely underlie the increase in apoptotic cell death found in aged Sox10-Cp^{KO} mice. The number of mature Cp^{KO} OLs that were caspase-3-positive significantly increased in both 10 and 12-month-old mice. This rise in apoptotic OLs is likely responsible for the drop in the density of myelinating OLs and for the demyelination of old Sox10-Cp^{KO} brains.

Interestingly, the CNS of 12 month-old Sox10-Cp^{KO} animals showed

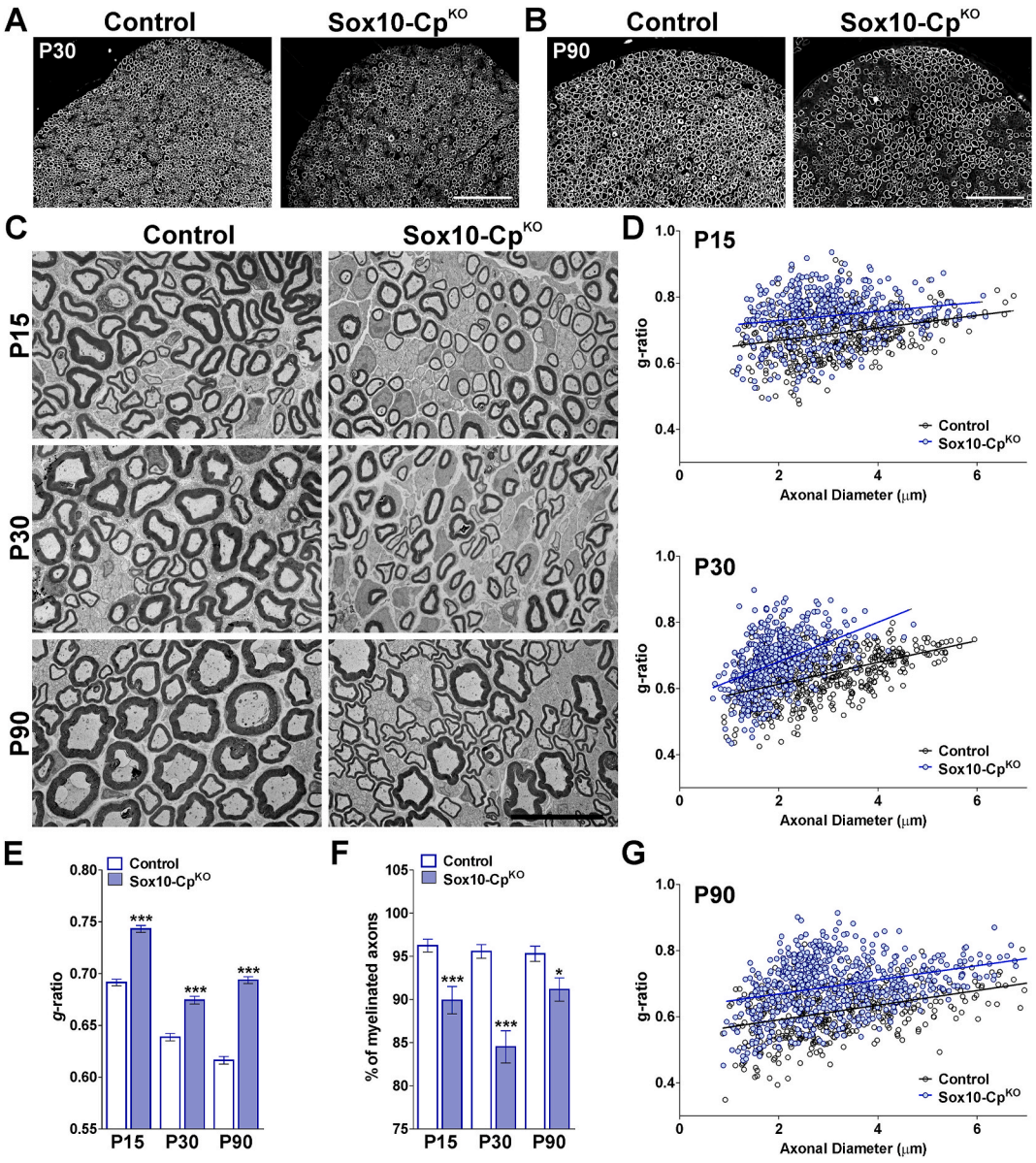

Fig. 10. *Electron microscopy of Cp^{KO} sciatic nerves.* (**A, B and C**) Semi-think sections and electron micrographs of axons in the sciatic nerve of control and Sox10-Cp^{KO} mice at different postnatal time points. Scale bar = 180 μm, semi-think; 6 μm, EM. (**D and G**) Scatter plot of *g*-ratio values of control and Sox10-Cp^{KO} mice at P15, P30 and P90. The lines represent the regression equation with 95% confidence intervals. (**E and F**) Mean *g*-ratio values and percentage of myelinated axons in control and Sox10-Cp^{KO} animals. Values are expressed as mean ± SEM. *$p < 0.05$, ***$p < 0.001$ versus respective controls.

a significant intensification in the number and staining intensity of iron-positive cells with the morphology and anatomical distribution of OLs. In contrast, the iron content of cortical neurons was found to be normal. These results suggest a specific oligodendroglia iron overload and indicate that Cp is crucial for iron homeostasis in aged OLs. Appropriate Cp ferroxidase activity is essential since only ferric iron (Fe^{3+}), but not ferrous iron (Fe^{2+}), can be incorporated into transferrin in the cerebrospinal fluid and interstitial fluid and acquired by neurons, astrocytes, and OLs [16]. The loss of Cp activity in old OLs can significantly increase the concentration of ferrous iron and reduce the amount of transferrin-bound ferric iron in the brain parenchyma. As a result, the incorporation of non-transferrin-bound iron by OLs or other brain cells can be abnormally high [44,45]. In addition, this toxic iron might not be released by Cp-deficient OLs because of the increased extracellular ferrous iron concentrations. All the above factors can potentially trigger excessive intracellular iron accumulation, oxidative stress, and apoptotic cell death in aged OLs. Furthermore, toxic ferrous iron released by Cp deficient OLs can produce oxidative stress and free radical formation and activate a cascade of pathological events leading to axonal degeneration and neuronal cell death. We have found signs of oxidative stress and neuronal cell loss in aged Sox10-Cp^{KO} brains. A significant reduction in the density of neurons and cortical thickness was evident in the somatosensory cortex of Sox10-Cp^{KO} mice at 12 months of age, and we detected an intensification in 8-OHdG DNA and RNA oxidation in cortical OLs and neurons. Thus, OL and neuronal oxidative stress, as well as oxidative myelin injury, can be accountable for the demyelination of aged Cp^{KO} mice.

SCs express high levels of Cp and it has been suggested that this protein plays a central role in the regulation of iron levels in the peripheral nervous system [20,21]. The presence of Cp on the plasma membrane of SCs may reflect an involvement of this protein in iron export during SC development and/or myelination. We have found that Cp ablation significantly disrupts SC maturation and myelination. Knocking-out Cp in SCs during early development diminished the

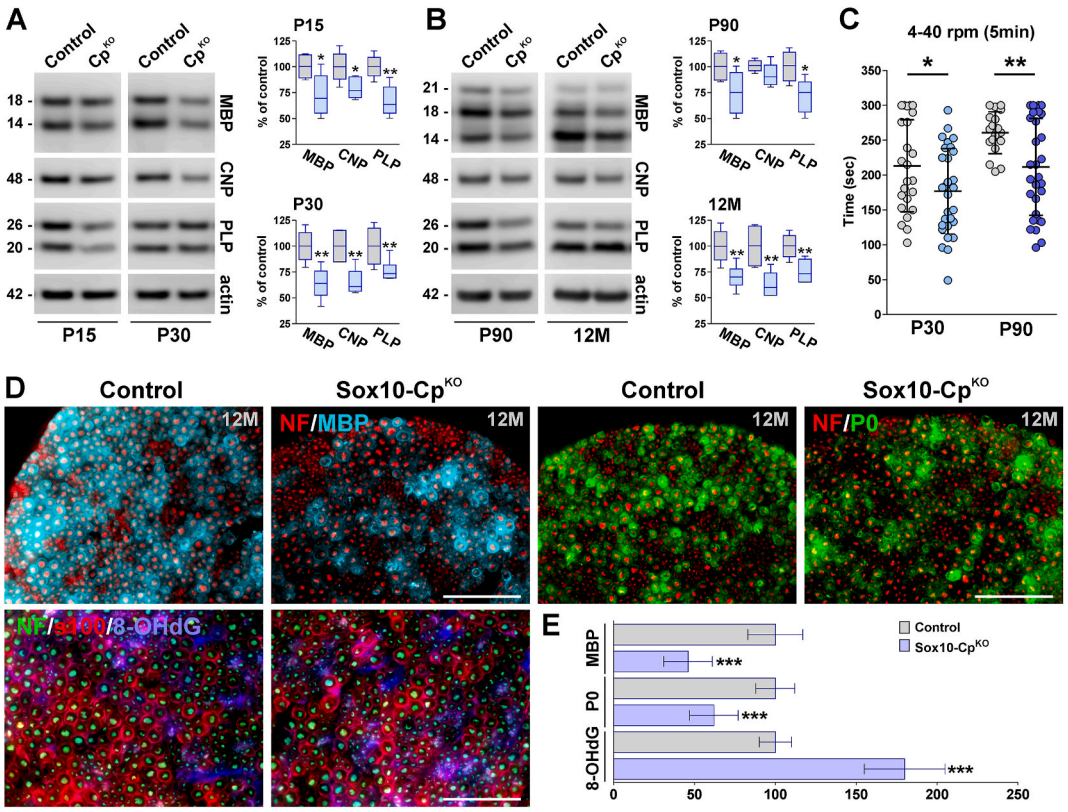

Fig. 11. *Expression of myelin proteins in Cp^{KO} sciatic nerves.* (**A and B**) Representative western blots for MBP, CNP and PLP made with total proteins purified from the sciatic nerve of controls and Sox10-Cp^{KO} mice at different time-points. Actin was used as the internal standard and box-and-whisker plots are showing means ± SD. *p < 0.05, **p < 0.01 vs. respective controls. (**C**) The latency to fall off the rotarod was measured in controls and Sox10-Cp^{KO} mice at P30 and P90. The speed of rotation was gradually increased from 4 to 40 rpm in a 5min interval (4–40 rpm). At least 15 mice were tested in each experimental group. Values are expressed as mean ± SD. *p < 0.05, **p < 0.01 versus respective controls. (**D**) MBP, P0, s100β, neurofilament M (NF) and 8-OHdG immunostaining in 12-month-old Sox10-Cp^{KO} sciatic nerves. Representative coronal sections are shown. Scale bar = 180 μm. (**E**) MBP, P0 and 8-OHdG expression was quantified by analyzing the integrated fluorescence intensity. Values are expressed as percentage of control values ± SEM. ***p < 0.001 vs. respective controls.

percentage of myelinated axons and myelin thickness in sciatic nerves. These changes were also detected in P90 and 12 month-old sciatic nerves in which Cp was deleted in mature myelinating SCs. Importantly, these myelin abnormalities produced significant motor coordination deficits at both P30 and P90. This phenotype suggests that, in the peripheral nervous system, Cp activity is essential for the normal maturation of SCs as well as for the function of mature myelinating SCs.

More experiments are needed to examine the consequences of Cp deletion in SC iron metabolism; for instance, we have not tested iron concentrantions in peripheral nerves during development. Thus, it is possible that Cp deletion induces oxidative stress and/or iron overload in immature SCs; however, as in the CNS, we have found evidence of oxidative stress in aged Cp^{KO} sciatic nerves. SCs are particularly susceptible to oxidative damage [46], and nerve damage due to oxidative stress and mitochondrial dysfunction are key pathogenic mechanisms involved in peripheral neuropathies [47]. Thus, it is possible that without proper Cp levels, SCs may experience an increase in free cytoplasmic iron, free radical formation, and oxidative stress. In summary, we have found that Cp activity is necessary for postnatal OL and SC maturation as well as for the function of both myelinating cell types in aged mice. Our results suggest a central role for Cp, and thus iron efflux, in OL and SC iron balance. This is pertinent to understanding iron homeostasis in both the central and peripheral nervous systems and developing novel therapies for neurodegenerative diseases in which iron accumulation and oxidative stress play a role.

Declaration of competing interest

The authors declare no competing financial interests.

Acknowledgements

National Institute of Neurological Disorders and Stroke (award number: R01NS07804) and startup package from the Jacobs School of Medicine and Biomedical Sciences, University at Buffalo.

References

[1] B. Wang, X.P. Wang, Does ceruloplasmin defend against neurodegenerative diseases? Curr. Neuropharmacol. 16 (2018) 1–10.
[2] F. Ryan, J.G. Zarruk, L. Lößlein, S. David, Ceruloplasmin plays a neuroprotective role in cerebral ischemia, Front. Neurosci. 12 (2019) 988.
[3] H. Drakesmith, E. Nemeth, T. Ganz, Ironing out ferroportin, Cell Metabol. 22 (2015) 777–787.
[4] B.N. Patel, R.J. Dunn, S.Y. Jeong, Q. Zhu, J.P. Julien, S. David, Ceruloplasmin regulates iron levels in the CNS and prevents free radical injury, J. Neurosci. 22 (2002) 6578–6586.
[5] H. Miyajima, Y. Hosoi, in: M.P. Adam, H.H. Ardinger, R.A. Pagon, S.E. Wallace, L.J. H. Bean, K. Stephens, et al. (Eds.), "Aceruloplasminemia," in Gene Reviews (Internet), University of Washington), Seattle, WA, 1993-2018.
[6] T.A. Rouault, Iron metabolism in the CNS: implications for neurodegenerative diseases, Nat. Rev. Neurosci. 14 (2013) 551–564.
[7] K. Yoshida, K. Furihata, S. Takeda, A. Nakamura, K. Yamamoto, H. Morita, S. Hiyamuta, S. Ikeda, N. Shimizu, N. Yanagisawa, A mutation in the ceruloplasmin gene is associated with systemic hemosiderosis in humans, Nat. Genet. 9 (1995) 267–272.
[8] H. Miyajima, Y. Nishimura, K. Mizoguchi, M. Sakamoto, T. Shimizu, N. Honda, Familiar apoceruloplasmin deficiency associated blepharospasm and retinal degeneration, Neurology 37 (1987) 761–767.

[9] L.H. Vroegindeweij, J.G. Langendonk, M. Langeveld, M. Hoogendoorn, J.A. Kievit, D. Di Raimondo, J.H. Paul Wilson, J.W.A. Boon, New insights in the neurological phenotype of aceruloplasminemia in Caucasian patients, Park. Relat. Disord. 36 (2017) 33–40.
[10] G. Marchi, F. Busti, A.L. Zidanes, A. Castagna, D. Girelli, Aceruloplasminemia: a severe neurodegenerative disorder deserving an early diagnosis, Front. Neurosci. 13 (2019) 325.
[11] S. Kono, H. Miyajima, Molecular and pathological basis of aceruloplasminemia, Biol. Res. 39 (2006) 15–23.
[12] S. Kono, Aceruloplasminemia: an update, Int. Rev. Neurobiol. 110 (2013) 125–151.
[13] H. Miyajima, Aceruloplasminemia, Neuropathology 35 (2014) 83–90.
[14] B.N. Patel, S. David, A novel glycosylphosphatidylinositol-anchored form of ceruloplasmin is expressed by mammalian astrocytes, J. Biol. Chem. 272 (1997) 20185–20190.
[15] B.N. Patel, R.J. Dunn, S. David, Alternative RNA splicing generates a glycosylphosphatidylinositol-anchored form of ceruloplasmin in mammalian brain, J. Biol. Chem. 275 (2000) 4305–4310.
[16] Z.M. Qian, Y. Ke, Rethinking the role of ceruloplasmin in brain iron metabolism, Brain Res. Brain Res. Rev. 35 (2001) 287–294.
[17] S.Y. Jeong, S. David, Glycosylphosphatidylinositol-anchored ceruloplasmin is required for iron efflux from cells in the central nervous system, J. Biol. Chem. 278 (2003) 27144–27148.
[18] Y. Zhang, K. Chen, S.A. Sloan, M.L. Bennett, A.R. Scholze, S. O'Keeffe, H. P. Phatnani, P. Guarnieri, C. Caneda, N. Ruderisch, S. Deng, S.A. Liddelow, C. Zhang, R. Daneman, T. Maniatis, B.A. Barres, J.Q. Wu, An RNA-sequencing transcriptome and splicing database of glia, neurons, and vascular cells of the cerebral cortex, J. Neurosci. 34 (2014) 11929–11947.
[19] S. Marques, A. Zeisel, S. Codeluppi, D. van Bruggen, A. Mendanha Falcão, L. Xiao, H. Li, M. Häring, H. Hochgerner, R.A. Romanov, D. Gyllborg, A. Muñoz Manchado, G. La Manno, P. Lönnerberg, E.M. Floriddia, F. Rezayee, P. Ernfors, E. Arenas, J. Hjerling-Leffler, T. Harkany, W.D. Richardson, S. Linnarsson, G. Castelo-Branco, Oligodendrocyte heterogeneity in the mouse juvenile and adult central nervous system, Science 352 (2016) 1326–1329.
[20] J.L. Salzer, L. Lovejoy, M.C. Linder, C. Rosen, Ran-2, a glial lineage marker, is a GPI-anchored form of ceruloplasmin, J. Neurosci. Res. 54 (1998) 147–157.
[21] J. Wolbert, X. Li, M. Heming, A.K. Mausberg, D. Akkermann, C. Frydrychowicz, R. Fledrich, L. Groeneweg, C. Schulz, M. Stettner, N. Alonso Gonzalez, H. Wiendl, R. Stassart, G.M. zu Hörste, Redefining the heterogeneity of peripheral nerve cells in health and autoimmunity, Proc. Natl. Acad. Sci. U.S.A. 117 (2020) 9466–9476.
[22] W.C. Skarnes, B. Rosen, A.P. West, M. Koutsourakis, W. Bushell, V. Iyer, A. O. Mujica, M. Thomas, J. Harrow, T. Cox, D. Jackson, J. Severin, P. Biggs, J. Fu, M. Nefedov, P.J. de Jong, A.F. Stewart, A. Bradley, A conditional knockout resource for the genome-wide study of mouse gene function, Nature 474 (2011) 337–342.
[23] I.A. McKenzie, D. Ohayon, H. Li, J.P. de Faria, B. Emery, K. Tohyama, W. D. Richardson, Motor skill learning requires active central myelination, Science 346 (2014) 318–322.
[24] X. Zhu, R.A. Hill, D. Dietrich, M. Komitova, R. Suzuki, A. Nishiyama, Age-dependent fate and lineage restriction of single NG2 cells, Development 138 (2011) 745–753.
[25] F.W. Farley, P. Soriano, L.S. Steffen, S.M. Dymecki, Widespread recombinase expression using FLPeR (Flipper) mice, Genesis 28 (2000) 106–110.
[26] V.T. Cheli, D.A. Santigo Gonzalez, L.N. Marziali, N.N. Zamora, M.E. Guitart, V. Spreuer, J.M. Pasquini, P.M. Paez, The divalent metal transporter 1 (DMT1) is required for iron uptake and normal development of oligodendrocyte progenitor cells, J. Neurosci. 38 (2018) 9142–9159.
[27] R. Wan, V.T. Cheli, D.A. Santiago González, Q. Wan, S.L. Rosenblum, P.M. Paez, Impaired postnatal myelination in a conditional knock-out mouse for the ferritin heavy chain in oligodendrocyte progenitor cells, J. Neurosci. 40 (2020) 7609–7624.
[28] V.T. Cheli, D.A. Santiago González, T. Namgyal Lama, V. Spreuer, V. Handley, G. G. Murphy, P.M. Paez, Conditional deletion of the L-type calcium channel Cav1.2 in oligodendrocyte progenitor cells affects postnatal myelination in mice, J. Neurosci. 36 (2016) 10853–10869.
[29] D.A. Santiago González, V.T. Cheli, N.N. Zamora, T. Namgyal Lama, V. Spreuer, G. G. Murphy, P.M. Paez, Conditional deletion of the L-type calcium channel Cav1.2 in NG2 positive cells delay remyelination in mice, J. Neurosci. 37 (2017) 10038–10051.
[30] K.B.J. Franklin, G. Paxinos, The Mouse Brain in Stereotaxic Coordinates, vol. 3, New York Academic Press, 2008.
[31] H. Kasai, S. Nishimura, Hydroxylation of the C-8 position of deoxyguanosine by reducing agents in the presence of oxygen, Nucl. Acids Symp. 12 (1983) 165–167.
[32] Z.L. Harris, Y. Takahashi, H. Miyajima, M. Serizawa, R.T. MacGillivray, Aceruloplasminemia: molecular characterization of this disorder in iron metabolism, Proc. Natl. Acad. Sci. U.S.A. 92 (1995) 2539–2543.
[33] Z.L. Harris, L.W. Klomp, J.D. Gitlin, Aceruloplasminemia: an inherited neurodegenerative disease with impaired iron homeostasis, Am. J. Clin. Nutr. 67 (1998) 972S–977S.
[34] H. Morita, S. Ikeda, K. Yamamoto, S. Morita, K. Yoshida, S. Nomoto, M. Kato, N. Yanagisawa, Hereditary ceruloplasmin deficiency with hemosiderosis: a clinicopathological study of a Japanese family, Ann. Neurol. 37 (1995) 646–656.
[35] N. Okamoto, S. Wada, T. Oga, Y. Kawabata, Y. Baba, D. Habu, Z. Takeda, Y. Wada, Hereditary ceruloplasmin deficiency with hemosiderosis, Hum. Genet. 97 (1996) 755–758.
[36] Y. Takahashi, H. Miyajima, S. Shirabe, S. Nagataki, A. Suenaga, J.D. Gitlin, Characterization of a nonsense mutation in the ceruloplasmin gene resulting in diabetes and neurodegenerative diseases, Hum. Mol. Genet. 5 (1996) 81–84.
[37] J.D. Gitlin, Aceruloplasminemia, Pediatr. Res. 44 (1998) 271–276.
[38] Z.L. Harris, A.P. Durley, T.K. Man, J.D. Gitlin, Targeted gene disruption reveals an essential role for ceruloplasmin in cellular iron efflux, Proc. Natl. Acad. Sci. U.S.A. 96 (1999) 10812–10817.
[39] S.Y. Jeong, S. David, Age-related changes in iron homeostasis and cell death in the cerebellum of ceruloplasmin-deficient mice, J. Neurosci. 26 (2006) 9810–9819.
[40] K. Schulz, C.D. Vulpe, L.Z. Harris, S. David, Iron efflux from oligodendrocytes is differentially regulated in gray and white matter, J. Neurosci. 31 (2011) 13301–13311.
[41] K.J. Smith, R. Kapoor, P.A. Felts, Demyelination: the role of reactive oxygen and nitrogen .species, Brain Pathol. 9 (1999) 69–92.
[42] M.K. Giacci, C.A. Bartlett, N.M. Smith, K.S. Iyer, L.M. Toomey, H. Jiang, P. Guagliardo, M.R. Kilburn, M. Fitzgerald, Oligodendroglia are particularly vulnerable to oxidative damage after neurotrauma in vivo, J. Neurosci. 38 (2018) 6491–6504.
[43] A.D. Roth, M.T. Núñez, Oligodendrocytes: functioning in a delicate balance between high metabolic requirements and oxidative damage, Adv. Exp. Med. Biol. 949 (2016) 167–181.
[44] C.A. Reilly, S.D. Aust, Stimulation of the ferroxidase activity of ceruloplasmin during iron loading into ferritin, Arch. Biochem. Biophys. 347 (1997) 242–248.
[45] M.E. Van Eden, S.D. Aust, Intact human ceruloplasmin is required for the incorporation of iron into human ferritin, Arch. Biochem. Biophys. 381 (2000) 119–126.
[46] C. Park, E.O. Choi, G.Y. Kim, H.J. Hwang, B.W. Kim, Y.H. Yoo, H.T. Park, Y. H. Choi, Protective effect of baicalein on oxidative stress-induced DNA damage and apoptosis in RT4-D6P2T Schwann cells, Int. J. Med. Sci. 16 (2019) 8–16.
[47] A. Areti, V.G. Yerra, V. Naidu, A. Kumar, Oxidative stress and nerve damage: role in chemotherapy induced peripheral neuropathy, Redox Biol. 2 (2014) 289–295.